Magnetic Susceptibilities of Transition Elements in Host Crystals. I. V^{3+} in Corundum*

WILLIAM H. BRUMAGE, C. RICHARD QUADE,† AND CHUN C. LIN‡
Department of Physics, University of Oklahoma, Norman, Oklahoma
(Received 20 March 1963)

The magnetic susceptibilities of V^{3+}-doped corundum crystals have been measured along and perpendicular to the trigonal crystalline axis over the temperature range of 4–500°K. A Faraday balance and a torsional balance were used to measure the absolute and anisotropy susceptibilities, respectively. Theoretical expressions for the magnetic susceptibilities as functions of temperature are obtained by employing the crystal-field approximation in the usual manner. The data of the optical spectrum fix the cubic-field parameter and the mixing ratio of the ^3F and ^3P states. The observed values of the magnetic susceptibilities follow a Curie-Weiss law over the temperature range of 77–500°K. Using 1.915 for $g_{\parallel}$ from the ESR (electron spin resonance) experiment, we obtain $g_{\perp}=1.720\pm0.005$ from the ratio of the slopes of the graphs of χ_i versus $(T+\theta_i)^{-1}$. The difference in the Van Vleck temperature-independent terms for $\chi_{\perp}$ and $\chi_{\parallel}$ which was evaluated by extrapolating the data to $T=\infty$, gives the trigonal splitting of the ground state as 1100 ± 100 cm^{-1}. At temperatures below 30°K the magnetic anisotropy becomes considerably larger and deviations from the Curie-Weiss law are found for both $\chi_{\parallel}$ and $\chi_{\perp}$. The zero-field splitting of the ground $^3A_2$ state is determined from the temperature dependence of the magnetic anisotropy as 8.4 cm^{-1}. The g values and the zero-field splitting provide an estimate of 95 cm^{-1} for the spin-orbit coupling constant. Finally by combining the trigonal splitting of the ground state determined from this work with that of the $^3T_1(P)$ state observed in the optical spectrum, an estimate of the two trigonal field parameters is obtained. Discussions of the crystal-field parameters in terms of the ligand bonding and the point-change model of the crystal are given.

I. INTRODUCTION

RECENT work on the optical absorption spectra and the electron spin resonance (ESR) experiments of the dilute crystalline salts of the transition elements has provided much information about the energy levels, the crystalline field, and the possible distortion of the geometry of the crystals due to the impurity substitution.[1–5] For instance, in the case of the vanadium (V^{3+})-doped corundum crystals, the crystalline structure is primarily cubic with a small trigonal distortion[1,3] with electronic energy levels as shown in Fig. 1. The $^3T_1$ state in the cubic field is split by the trigonal field into $^3A_2$ and ^3E levels with energy spacing Δ_T. The spin-orbit coupling further splits the ground $^3A_2$ state into two components separated by δ, the zero-field splitting. The two parameters Δ_T and δ have been determined from the electron spin resonance absorption and from the optical spectra.[1–6] From the magnitudes of such crystal-field parameters along with the intensities of the optical spectral bands for several transition metal ions in corundum single crystals, McClure was able to examine the validity of the point-charge model of the crystal-field theory as well as the possibility of a slight shift of the sites of the impurity cations.[1] However, in most of the experiments, Δ_T and δ are generally determined from the temperature variations of the absorption intensity of the ESR and optical spectra. The difficulty of intensity measurements has greatly limited the accuracy of the values of these parameters. Thus, Δ_T was given as 280 to 400 cm^{-1} from the ESR data in contrast to the optical result of 960 to 1200 cm^{-1}. In this

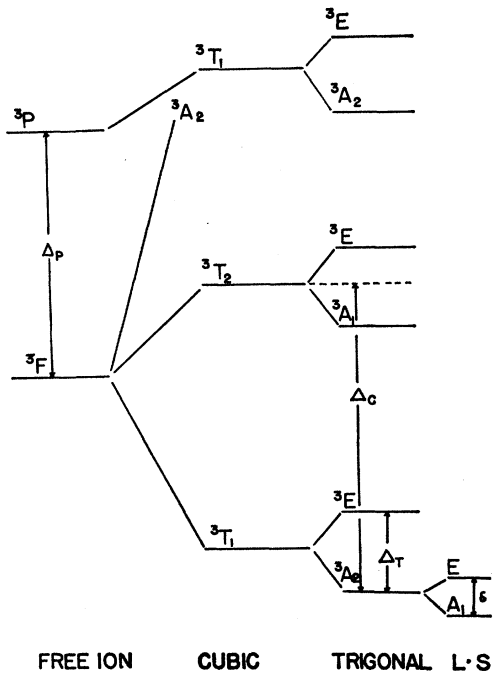

FIG. 1. Energy levels of V^{3+} in a trigonal field.

* Supported by the U. S. Office of Naval Research.
† National Science Foundation Predoctoral Fellow, 1959–1962. Present address: Department of Physics, University of Delaware, Newark, Delaware.
‡ Alfred P. Sloan Foundation Fellow.
[1] D. S. McClure, J. Chem. Phys. **36**, 2757 (1962).
[2] H. A. Weakliem, J. Chem. Phys. **36**, 2117 (1962); H. A. Weakliem and D. S. McClure, Suppl. J. Appl. Phys. **33**, 347 (1962).
[3] M. H. L. Pryce and W. A. Runciman, Discussions Faraday Soc. **26**, 35 (1958).
[4] G. M. Zverev and A. M. Prokhorov, Zh. Eksperim. i Teor. Fiz. **34**, 1033 (1958); **38**, 449 (1960); **40**, 1016 (1961) [translations: Soviet Phys.—JETP **7**, 707 (1958); **11**, 330 (1960); **13**, 714 (1961)].
[5] D. K. Rei, Fiz. Tverd. Tela **3**, 2214 (1961) [translation: Soviet Phys.—Solid State **3**, 1606 (1962)].
[6] S. Foner and W. Low, Phys. Rev. **120**, 1585 (1960).

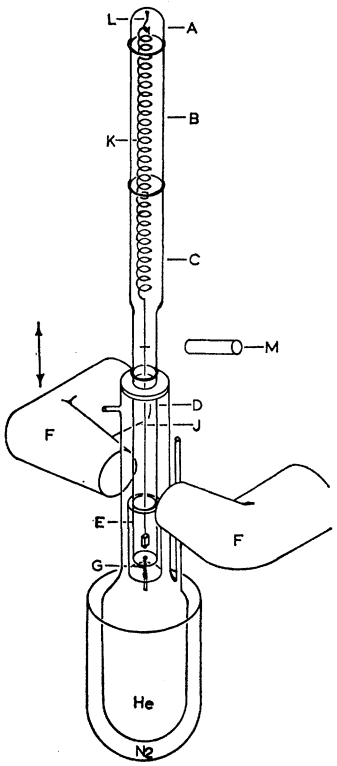

FIG. 2. Diagram of the Faraday balance.

paper we shall describe the use of the dependence of the magnetic susceptibilities on temperature to determine the crystal-field parameters. We have measured the magnetic susceptibilities of the V^{3+}-doped corundum crystals from liquid-helium temperature to 500°K along and perpendicular to the trigonal axis, from which Δ_T and δ are evaluated. Also an estimate of the spin-orbit coupling constant is obtained.

The magnetic properties of pure V_2O_3 have been investigated by several authors. The pure vanadium sesquioxide crystal becomes antiferromagnetic[7] at 168°K. The use of diluted crystals makes it possible to study the paramagnetism at lower temperatures and provide more information about the crystalline field.

The magnetic susceptibility of vanadium alum has been investigated by Siegert and by van den Handel and Siegert.[8] Their measurements were made only for the average susceptibilities over the three crystalline axes. From the analysis of magnetic data, Siegert and van den Handel have obtained a set of values for Δ_T and δ. Although the accuracy of the two parameters reported by these authors is limited by the fact that all the susceptibility measurements were made below 300°K and that the mixing between the ^3F and ^3P states (see Sec. III) has been neglected in Siegert's theory, their results do lead to the significant conclusion that in vanadium alum the ground state resulting from the trigonal field splitting is the $^3A_2$.

[7] G. Foex, J. Phys. Radium **12**, 156 (1951).
[8] A. Siegert, Physica **4**, 138 (1937); J. Van den Handel and A. Siegert, Physica **4**, 871 (1937).

II. EXPERIMENT

The crystals of the V^{3+}-doped corundum were furnished by McClure.[1] Crystals of two different concentrations (0.092% and 0.73%) have been used in our measurements. The susceptibilities of both crystals have been measured for temperatures above 77°K. At lower temperature, the susceptibilities become so large that only the diluted sample was used.

The magnetic susceptibilities along the crystalline axes were measured by a Faraday balance. At very low temperature the magnetic anisotropy becomes so large that the geometrical configuration in which the trigonal axis of the crystal lies parallel to the magnetic field, is unstable. Thus, we have measured $\chi_\perp$ from 500°K down to liquid-helium temperature, but measurements of $\chi_\parallel$ are limited only to temperature above 12°K. Below this temperature $\chi_\parallel$ is obtained from direct measurements of $\chi_\perp - \chi_\parallel$ by means of an anisotropy torsion balance. Descriptions of the Faraday balance and the anisotropy balance are given in the following paragraphs.

1. Faraday Balance

A schematic diagram of the Faraday balance[9,10] used in this experiment is shown in Fig. 2. The upper portion (A, B and C) is made of glass with two O-ring seals and one ground glass seal placed at several positions for easy assembly. The lower segment (D) is constructed of stainless-steel tubing with a thick copper tube (E) at the very bottom to which are attached two thermocouples. The entire system is usually evacuated and helium exchange gas admitted at a pressure of 2–4 cm of Hg. A small heater coil (G) is placed around the copper tube which is surrounded by a stainless-steel jacket. A calibrated quartz spring (K) (force constant ~2 mg/mm) is attached to a hook (L) at the top end and the sample is attached to the lower end by means of a sample holder (J) made of a thin quartz fiber. A measuring microscope (M) is used to determine the extension of the spring.

The nonhomogeneous magnetic field is supplied by a 2700-G General Electric magnet assembly (F). The magnet is moved past the sample in the vertical direction by the use of a motor driven lift to which the base of the magnet has been bolted. A reversing switch allows the magnet to move both up and down.

A specially designed helium Dewar was constructed for low-temperature work. The helium, liquid or cold helium gas, is admitted through a side tube from a 25-liter storage Dewar by means of a helium transfer tube. Liquid nitrogen is used from 77–300°K. In order to

[9] P. W. Selwood, *Magnetochemistry* (Interscience Publishers, Inc., New York, 1956), 2nd ed.
[10] L. F. Bates, *Modern Magnetism* (Cambridge University Press, New York, 1961), 4th ed.

obtain temperatures in the range 300–500°K, the bottom part of the balance is removed and a heater, constructed of copper tubing and wound with resistance wire, is attached at one of the joints.

The temperature is measured by the copper-Constanan thermocouples in conjunction with a calibrated Leeds and Northrup K-3 potentiometer. The thermocouple voltage gives the temperature of the copper tube (E in Fig. 2) which is assumed to be at the same temperature as the crystal. That the crystal and the copper tube are in thermal equilibrium with each other has been demonstrated by Stout and Griffel in a similar apparatus.[11] As a further check of the accuracy of the temperature measurements, we have measured the magnetic susceptibilities of Cr^{3+}:MgO over the range of 6–293°K and of Cr_2O_3:Al_2O_3 from 293–500°K. A plot of χ versus T^{-1} gave a straight line in each case.

In calibrating the magnetic field it was not necessary to obtain $\mathfrak{H}$, but instead $\mathfrak{H}(d\mathfrak{H}/dz)$. A piece of pure platinum (86.5 mg), 1-mm diam and 5 mm long, was placed horizontally on the balance in place of the sample. The deflection of the spring was determined as the magnet swept past at millimeter intervals. Using the equation

$$kd = m\chi\mathfrak{H}(d\mathfrak{H}/dz) \qquad (1)$$

and a value of 0.969×10^{-6} for the mass susceptibility of the platinum,[12] we have determined $\mathfrak{H}(d\mathfrak{H}/dz)$ at each millimeter interval from which the effective value of $\mathfrak{H}(d\mathfrak{H}/dz)$ could be determined for a sample of any length. To check the consistency of these values the piece of platinum was placed in the balance in a vertical position and the susceptibility measured. This was also repeated with another piece of platinum. The results of our measurement differed from the accepted value only in the fourth place which is within the uncertainty of the readings of the spring deflection. Other known samples such as copper sulfate and glycerin were tried and the susceptibilities as determined by our method proved to be within 1% of the accepted values.

In measuring the susceptibility the V_2O_3:Al_2O_3 sample was placed in the holder and then the apparatus assembled. One of the magnetic axes of the crystal was lined up parallel to the magnetic field. The magnet was then moved vertically until a maximum deflection was observed. The fixed cross hair in the microscope was aligned with a fixed mark on the sample holder. The magnet was then moved until a maximum deflection

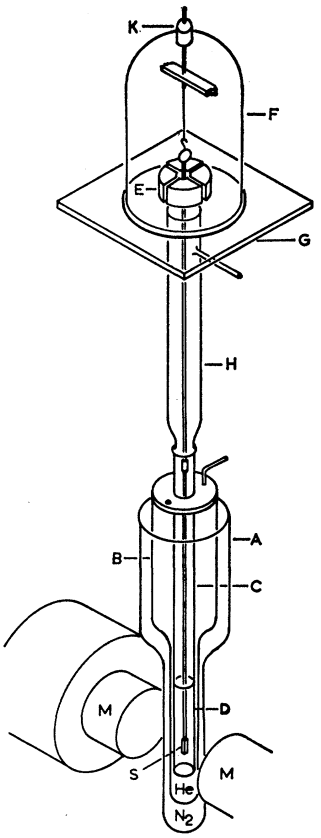

FIG. 3. Diagram of the anisotropy torsion balance.

TABLE I. Magnetic susceptibilities (per gram sample) of V^{3+}-doped corundum.

Sample A. Concentration (0.73%)			
T (°K)	$\chi_{\parallel}\times10^{7}$ (cgs emu)	T (°K)	$\chi_{\perp}\times10^{7}$ (cgs emu)
77.3	4.70	77.3	4.08
88.0	3.68	88.0	3.23
91.0	3.49	103	2.26
121	1.92	109	1.96
127	1.68	118	1.60
138	1.25	130	1.11
145	1.04	137	0.89
155	0.75	145	0.72
156	0.73	154	0.49
202	−0.26	174	0.15
272	−0.93	217	−0.46
290	−1.14	253	−0.84
296	−1.16	296	−1.17
470	−1.96	430	−1.68
507	−2.11	501	−1.88
Sample B. Concentration (0.092%)			
T (°K)	$\chi_{\parallel}\times10^{7}$ (cgs emu)	T (°K)	$\chi_{\parallel}\times10^{7}$ (cgs emu)
295	−3.25	96	−2.61
282	−3.23	77.3	−2.39
134	−2.88	12.2	1.23
T (°K)	$\chi_{\perp}\times10^{-7}$ (cgs emu)	T (°K)	$\chi_{\perp}\times10^{-7}$ (cgs emu)
295	−3.28	21.5	0.11
179	−3.12	18.6	0.80
125	−2.91	18.0	1.08
95	−2.70	16.0	1.50
77.3	−2.53	9.8	4.15
58	−2.32	8.25	6.70
56	−2.16	8.10	7.12
43.3	−1.65	6.70	8.72
35.9	−1.48	6.60	9.36
32.9	−0.95	5.4	12.00

[11] J. W. Stout and M. Griffel, J. Chem. Phys. **18**, 1449 (1950).

[12] F. E. Senftle, M. D. Lee, A. A. Monkewicz, J. W. Mayo, and T. Pankey, Rev. Sci. Instr. **29**, 429 (1958).

TABLE II. Magnetic anisotropy (per gram sample) of V^{3+}-doped corundum.

Sample B. Concentration (0.092%)			
T (°K)	$\Delta\chi\times10^6$ (cgs emu)	T (°K)	$\Delta\chi\times10^6$ (cgs emu)
4.2	1.300	16.4	0.105
4.3	1.247	16.9	0.083
8.1	0.523	17.4	0.077
8.5	0.431	22.2	0.037
8.65	0.395	23.4	0.028
9.2	0.362	24.5	0.021
10.5	0.248	25.3	0.018
11.1	0.233	26.3	0.016
13.3	0.161	27.1	0.012
13.9	0.137	29.4	0.008
14.7	0.120	35.0	−0.001

was observed in the opposite direction. The deflection was read from the scale of the microscope. From the known values of k, d, m, and $\mathfrak{H}(d\mathfrak{H}/dz)$ along with Eq. (1), the susceptibility at this temperature could be determined. By varying the amount of heater current, the flow of liquid, or the flow of the cooled gas, a new temperature was obtained and the process repeated to measure the susceptibility at the new temperature. Table I gives the results obtained in this manner for $\chi_{\parallel}$ and $\chi_{\perp}$ at different temperatures for the two V_2O_3:Al_2O_3 crystals.

2. Anisotropy Torsion Balance

To measure the difference in susceptibility of a sample at low temperatures, a torsion balance[9] (shown in Fig. 3) was constructed. The homogeneous magnetic field is supplied by a rotating Varian 6-in. magnet (M) and its regulated power supply. The gap is set at 2.85 in. to accommodate a liquid-helium assembly used in ESR measurements. The helium Dewar (B) and nitrogen Dewar (A) are used as supplied, but in place of the waveguide assembly, a different unit is used. It has the same dimensions as the waveguide assembly but the waveguide itself is replaced by a round tube. The upper portion (C) of the tube is made of stainless steel while the bottom is a thick copper tube (D) to which a copper-Constanan thermocouple and a gold-cobalt versus silver-gold thermocouple are cemented directly opposite the sample.

A magnetically anisotropic sample in a homogeneous field experiences a torque which is proportional to $\chi_{\perp}-\chi_{\parallel}$. Instead of finding this torque from the angle of torsional rotation, we applied a counter torque to bring the crystal back to the original orientation. The counter torque was supplied by a quadrant electrometer (E in Fig. 3). The difference of potential between the quadrants and the potential of the vane is kept constant during a series of measurements. The zero of the electrometer can be changed by means of a ball and socket joint (K) at the top of the bell jar (F) which was placed over the electrometer. A telescope and scale are used to detect the deflection of the vane. The bell jar rests on a rubber pad which, in turn, is supported by an aluminum plate (G). Electrical leads to the electrometer pass through the aluminum plate from two batteries. One of the batteries supplies 300 V to the vane while the other battery is able to supply either 1.4, 6, 22, 45, or 90 V to the quadrants. In this experiment, the voltage applied to the quadrants can be kept constant and the magnetic field changed to produce a zero deflection or it is also possible to fix the magnetic field and change the voltages applied to the electrometer by means of a battery and a potentiometer.

The aluminum plate is connected to the Dewar assembly by means of a glass tube (H) which has O-ring seals on both ends. The glass tube also has an opening for evacuation purposes and helium exchange gas can be admitted at any desired pressure. The supports for the Dewar system and the electrometer assembly are not shown in Fig. 3.

The sample (S) is supported by a very thin quartz holder. The holder is connected to the bottom of a very long quartz rod (2-mm diam). The upper end of the quartz rod is, in turn, cemented to the vane of the electrometer. The quartz rod consists of two parts for ease of handling.

The procedure for making the measurements consisted of the following. The sample was placed in the holder and the balance assembled. The balance was then evacuated and helium gas was admitted until the pressure reached 4 cm Hg. The positive terminal of the 300-V battery was connected to the vane terminal on the electrometer and the negative terminal grounded. The quadrants were also grounded. By means of the manual control at the top of the bell jar the electrometer was adjusted for zero reading on the scale. The magnet was turned on and then rotated until a maximum deflection is noted on the scale. The magnet is then fixed in this position.

For the first series of measurements, a difference of potential was applied to the quadrants. In the case of the V_2O_3:Al_2O_3 sample a 22 V battery was used in the 4–35°K range. The magnetic field was then adjusted until a zero deflection was observed in the telescope. The current through the magnet was determined by the meter on the regulated power supply. The temperature was determined by the use of the thermocouple and K-3 potentiometer. The temperature of the sample was then varied and the same process repeated.

Bates gives the equation for the torque acting on a sample in a homogeneous magnet field as[10]

$$L=m(\Delta\chi)\mathfrak{H}^2\sin2\theta. \qquad (2)$$

If the voltages applied to the electrometer are kept constant, then the counter torque should be the same for each measurement. Since the sample is always rotated to the same position, we keep θ the same in each case. Therefore, $\mathfrak{H}^2\Delta\chi$ should be a constant. A plot of current versus $\mathfrak{H}$ for the magnet gives a straight line within the accuracy of the gaussmeter for the gap and

TABLE III. Magnetic anisotropy (per gram sample) of V^{3+}-doped corundum.

Sample B. Concentration (0.092%)			
T°K	$\Delta\chi\times10^6$	T°K	$\Delta\chi\times10^6$
4.2	1.330	7.6	0.533
4.5	1.165	8.1	0.457
4.7	1.091	8.9	0.405
4.9	1.058	9.2	0.342
4.95	1.030	9.7	0.304
5.2	0.990	10.5	0.257
5.3	0.943	11.0	0.250
5.45	0.924	11.2	0.209
5.6	0.861	13.5	0.148
5.8	0.840	14.1	0.143
5.95	0.790	14.5	0.112
6.5	0.715	16.2	0.095
7.05	0.615	17.6	0.074

magnetic fields used. It follows that

$$\Delta\chi_{T_1}/\Delta\chi_{T_2}=I_{T_2}^2/I_{T_1}^2. \quad (3)$$

Using the value of $\Delta\chi$ at 12.2°K as determined from the Faraday balance, one can determine $\Delta\chi$ for the other temperatures. These values are given in Table II.

For the other series of measurements the magnetic field was kept constant and the voltage applied to the quadrants was varied until a zero deflection was observed. The voltage was measured by a voltmeter. The temperature of the sample was changed and the voltage measured for other temperatures.

Since the field and the angle θ in Eq. (2) was kept constant the counter torque is directly proportional to $\Delta\chi$. For an electrometer

$$L=cV_q(V_v-\tfrac{1}{2}V_q), \quad (4)$$

where V_q is the voltage applied to the quadrants, and V_v is the voltage applied to the vane and c is a constant. It follows that

$$(\Delta\chi)_{T_1}/(\Delta\chi)_{T_2}=V_q(V_v-\tfrac{1}{2}V_q)_{T_1}/V_q(V_v-\tfrac{1}{2}V_q)_{T_2}. \quad (5)$$

These values are given in Table III.

The constant field measurements are better in the 4–20°K range while the constant voltage measurements are better in the 20–40°K range.

III. THEORY

In our analysis of the magnetic susceptibility data, we will use crystal-field theory as a suitable model for the physical problem. It will be assumed that the crystalline field is primarily cubic with a small trigonal component. Further, it will be assumed that the unit cell has a center of inversion so that the symmetry group of the crystal is C_{3v}. It has been shown by McClure that any deviation from these assumptions is indeed small.[1]

The ground-state configuration for V^{3+} is $(d)^2$ with multiplets ^3F, ^1D, ^3P, ^1G, ^1S in order of increasing energy. The Hamiltonian which describes the effect of the crystal field will be assumed to have a dominant cubic term[13]

$$V_c=\sum_{i=1,2} r_i^4A_4^0\{Y_{4,0}(\theta_i,\phi_i)+(10/7)^{1/2}[Y_{4,3}(\theta_i,\phi_i)-Y_{4,-3}(\theta_i,\phi_i)]\}, \quad (6)$$

with a small trigonal component

$$V_t=\sum_{i=1,2}\{r_i^2B_2^0Y_{2,0}(\theta_i,\phi_i)+r_i^4B_4^0Y_{4,0}(\theta_i,\phi_i)\}. \quad (7)$$

It is well known from symmetry considerations that the cubic field partially removes the degeneracy of the multiplets:

$$^3F\rightarrow{}^3T_1+{}^3T_2+{}^3A_2,\quad {}^1D\rightarrow{}^1T_2+{}^1E,$$
$$^3P\rightarrow{}^3T_1,\qquad {}^1G\rightarrow{}^1T_1+{}^1T_2+{}^1E+{}^1A_1, \quad (8)$$
$$^1S\rightarrow{}^1A_1.$$

Further lifting of the degeneracy by the trigonal component causes the cubic levels to split:

$$T_1\rightarrow E+A_2,\quad T_2\rightarrow E+A_1, \quad (9)$$

with E, A_1, A_2 unchanged (see Fig. 1).

In addition to the crystalline potential, we must consider the spin-orbit coupling and the interaction with an external field $\mathfrak{H}$:

$$\lambda\mathbf{L}\cdot\mathbf{S}+\mu_0(\mathbf{L}+g_s\mathbf{S})\cdot\mathfrak{H}, \quad (10)$$

where λ is the spin-orbit coupling constant and μ_0 is the Bohr magneton. The calculation will be divided into two parts. In the first section we will obtain the matrix elements of the complete Hamiltonian,

$$H=H_0+V_c+V_t+\lambda\mathbf{L}\cdot\mathbf{S}+\mu_0(\mathbf{L}+g_s\mathbf{S})\cdot\mathfrak{H} \quad (11)$$

in the cubic-field representation, using as basis functions linear combinations of the free V^{3+} ion wave functions. Then in the second part the resulting secular equation will be solved in a manner suitable for the analysis of the experimental data. Here H_0 denotes the Hamiltonian of the free ion neglecting configuration interaction. The wave functions of the various multiplet components (such as ^3F) are taken as the usual Clebsch-Gordan type combinations of the one-electron orbitals,[14] while the multiplet separations are treated as parameters to be determined from the optical spectra.

This approach corresponds to what is termed the "weak-field approximation" in that the electrostatic forces between the electrons are included in the unperturbed Hamiltonian and the crystalline field is treated as a perturbation.[13] This procedure is most suitable for those systems where the crystal-field splittings are small compared to the spacings of the L multiplet. On the other hand, Pryce and Runcimann[3] used in their calculation of the energy levels of V^{3+} in corundum, the

[13] See, for example, D. S. McClure, Solid State Phys. **9**, 399 (1959); W. Moffitt and C. J. Ballhausen, Ann. Rev. Phys. Chem. **7**, 107 (1956).

[14] E. U. Condon and G. H. Shortley, *The Theory of Atomic Spectra* (Cambridge University Press, London, 1951).

TABLE IV. Cubic-field functions of ^3F and ^3P.[a]

^3F

$^3T_1$: $\Psi(^3T_1,-,M_s)=-[\psi(^3F,-1,M_s)+(5)^{1/2}\psi(^3F,2,M_s)]/\sqrt{6}$

$\Psi(^3T_1,0,M_s)=\frac{1}{3}\{2\psi(^3F,0,M_s)+(\frac{5}{2})^{1/2}[\psi(^3F,3,M_s)-\psi(^3F,-3,M_s)]\}$

$\Psi(^3T_1,+,M_s)=-[\psi(^3F,1,M_s)-(5)^{1/2}\psi(^3F,-2,M_s)]/\sqrt{6}$

$^3T_2$: $\Psi(^3T_2,+,M_s)=[(5)^{1/2}\psi(^3F,1,M_s)+\psi(^3F,-2,M_s)]/\sqrt{6}$

$\Psi(^3T_2,0,M_s)=[\psi(^3F,3,M_s)+\psi(^3F,-3,M_s)]/\sqrt{2}$

$\Psi(^3T_2,-,M_s)=[(5)^{1/2}\psi(^3F,-1,M_s)-\psi(^3F,2,M_s)]/\sqrt{6}$

$^3A_2$: $\Psi(^3A_2,M_s)=\frac{1}{3}\{(5)^{1/2}\psi(^3F,0,M_s)-\sqrt{2}[\psi(^3F,3,M_s)-\psi(^3F,-3,M_s)]\}$

^3P

$^3T_1$: $\Psi(^3T_1,+,M_s)=\psi(^3P,1,M_s)$

$\Psi(^3T_1,0,M_s)=\psi(^3P,0,M_s)$

$\Psi(^3T_1,-,M_s)=\psi(^3P,-1,M_s)$

[a] The notation ψ refers to the atomic wave functions of V^{3+}. The first symbol inside the parenthesis signifies the values of S and L, the second gives M_L, and the last, M_s. The cubic-field functions are denoted by Ψ with the first symbol inside the parentheses for the symmetry properties and the second as an index of the components of the degenerate states. The free-ion functions ψ are constructed from linear combinations of the products of one-electron d orbitals. The Clebsch-Gordan coefficients are taken to be those given in Condon and Shortley (Ref. 14).

strong-field approximation in which the $1/r_{12}$ interaction is treated as a perturbation on the cubic-field energy. Although our problem belongs more properly to the case of an intermediate field, we shall use the weak-field approximation as the starting point and set up the energy matrix in the representation where H_0 is diagonal. Upon solving the secular equations we then obtain the solutions for the intermediate field. The reasons for choosing this "weak-field representation" are as follows:

(1) For V^{3+} the two Slater-Condon parameters do not adequately account for the observed multiplet spacing of the free-ion, let alone in a crystal. The weak-field approximation allows the multiplet separations to be treated as parameters to be determined from the experimental data. A similar parametric approach cannot be taken for the strong-field approximation.

(2) The trigonal component of the crystal field is small compared to the multiplet spacings and cubic terms. Therefore, in the representation where the large terms are diagonal, only the first-order trigonal energy needs to be considered. In the strong-field approximation mixing by multiplet interactions causes off-diagonal trigonal matrix elements to contribute in first order. The usual assumption that these nondiagonal elements are zero is not necessarily a valid approximation.

The strong-field approximation does have the advantage that the effect of covalent bonding of the central ion with the ligands can be taken into consideration by forming LCAO of the V^{3+} ion (strong-field one-electron orbitals) with those of the ligands.[15–17] Indeed, it has been shown that the inclusion of the ligand orbitals might have a pronounced effect on the g shift and zero-field splitting.[18] However, in this work it is possible to fit the magnetic data by the simple crystal-field theory without explicitly introducing the ligand orbitals. The effect of the latter will be discussed in Sec. V.

1. Hamiltonian Matrix

The matrix elements of the Hamiltonian

$$H'=V_c+V_t \tag{12}$$

are easily evaluated using as a basis the functions of the cubic-field representation. These functions are linear combinations of the free-ion functions for the electronic configuration $(3d)^2$ and are listed in Table IV for the ^3F and ^3P states. Of course, the free-ion functions may be obtained from the products of one-electron d orbitals by utilizing the Clebsch-Gordan coefficients. The matrix elements for the cubic and trigonal crystalline potentials are listed in Table V. We shall use β as the cubic-field parameter which is related to the quantities in Eq. (6) as

$$\beta=-A_4{}^0\langle r^4\rangle/14\sqrt{\pi}. \tag{13}$$

In the case of a pure cubic field, β is equal to $(2/3)Dq$. Likewise, the two trigonal-field parameters γ and τ are defined as

$$\begin{aligned}\gamma&=-B_4{}^0\langle r^4\rangle/42\sqrt{\pi},\\ \tau&=-(\sqrt{5})B_2{}^0\langle r^2\rangle/140\sqrt{\pi},\end{aligned} \tag{14}$$

where $B_2{}^0$ and $B_4{}^0$ were introduced in Eq. (7). The behavior of the cubic levels as a function of the cubic-field parameter has been discussed by Orgel.[19]

It is well known[20] that in a trigonal field the ground $^3T_1$ splits in such a way that the $^3A_2$ level has lower energy than ^3E (Fig. 1). Further, the optical data of McClure[1] suggest that $^3A_2$ is also lower for the excited $^3T_1(^3P)$ state with splitting around 380 cm^{-1}. It has not been possible to determine directly the amount of trigonal splitting in the ground state, although McClure obtained a value of 960 cm^{-1} from the temperature dependence of the intensity of the optical spectrum.[1]

Addition of the spin-orbit coupling $\lambda\mathbf{L}\cdot\mathbf{S}$ further removes the degeneracy of the orbital ground state $(^3A_2\rightarrow E+A_1)$ with the A_1 level lowest. This splitting δ depends upon the spin-orbit coupling parameter λ and the trigonal splitting of $^3T_1(^3F)$, Δ_T. The matrix elements of

$$H''=\lambda\mathbf{L}\cdot\mathbf{S}+\mu_0(\mathbf{L}+g\mathbf{S})\cdot\mathfrak{H} \tag{15}$$

are listed in Table VI. The parameters α, α', and α'' in the matrix elements of Table VI are determined through the mixing of ^3F and ^3P by the cubic field. For zero mixing they would have the values 1.50, $\sqrt{2.50}$, and 1, respectively.

[15] K. W. H. Stevens, Proc. Roy. Soc. (London) **A219**, 542 (1953); J. Owen, Proc. Roy. Soc. (London) **A227**, 183 (1955).
[16] M. Tinkham, Proc. Roy Soc. (London) **A236**, 549 (1956).
[17] S. Koide and M. H. L. Pryce, Phil. Mag. **3**, 607 (1958).
[18] H. Kamimura, Phys. Rev. **128**, 1077 (1962).
[19] L. E. Orgel, J. Chem. Phys. **23**, 1004 (1955).
[20] J. H. Van Vleck, Discussions Faraday Soc. **26**, 96 (1958).

TABLE V. Energy matrix of the crystal field in the cubic representation.

$^3A_2$:	$^3T_1(^3F)$	$^3T_1(^3P)$	$^3A_2(^3F)$		
	$-9\beta+13\gamma+2\tau$	$-6\beta-8\gamma+16\tau$	$2(5)^{1/2}\gamma-4(5)^{1/2}\tau$		
		$\Delta(P)+28\tau$	$-4(5)^{1/2}\gamma+8(5)^{1/2}\tau$		
			$18\beta+14\gamma$		
^3E:	$^3T_1(^3F)$	$^3T_2(^3F)$	$^3T_1(^3P)$		
	$-9\beta-17\gamma-\tau$	$-4(5)^{1/2}\gamma+(5)^{1/2}\tau$	$-6\beta-3\gamma-8\tau$		
		$3\beta-\gamma-5\tau$	$3(5)^{1/2}\gamma+8(5)^{1/2}\tau$		
			$\Delta(P)-14\tau$		
$^3A_1$:	$^3T_2(^3F)$				
	$3\beta+9\gamma+10\tau$				
$^1A_1$:	$^1T_2(^1D)$	$^1T_2(^1G)$	$^1A_1(^1G)$	$^1A_1(^1S)$	
	$\Delta(D)-\frac{24}{7}\beta-\frac{72}{7}\gamma+\frac{60}{7}\tau$	$-\frac{30}{7}\sqrt{3}\beta-\frac{200}{21}\sqrt{3}\gamma-\frac{160}{21}\sqrt{3}\tau$	$-\frac{20}{21}(35)^{1/2}\gamma-\frac{16}{21}(35)^{1/2}\tau$	$28(10)^{1/2}\tau$	
		$\Delta(G)-\frac{39}{7}\beta-\frac{71}{21}\gamma-\frac{130}{7}\tau$	$-\frac{26}{21}(35)^{1/2}\gamma-\frac{20}{7}(35)^{1/2}\tau$	$-\frac{4}{3}(210)^{1/2}\gamma$	
			$\Delta(G)+6\beta+\frac{14}{3}\gamma$	$-6(6)^{1/2}\beta-\frac{14}{3}(6)^{1/2}\gamma$	
				$\Delta(S)$	
^1E:	$^1E(^1D)$	$^1T_2(^1D)$	$^1E(^1G)$	$^1T_2(^1G)$	$^1T_1(^1G)$
	$\Delta(D)+\frac{36}{7}\beta+4\gamma$	$\frac{20}{7}\sqrt{2}\gamma+\frac{30}{7}\sqrt{2}\tau$	$\frac{60}{7}\sqrt{3}\beta+\frac{20}{3}\sqrt{3}\gamma$	$\frac{40}{21}(6)^{1/2}\gamma+\frac{20}{7}(6)^{1/2}\tau$	$-\frac{10}{7}(14)^{1/2}\gamma+\frac{20}{7}(14)^{1/2}\tau$
		$\Delta(D)-\frac{24}{7}\beta+\frac{8}{7}\gamma-\frac{30}{7}\tau$	$-\frac{110}{21}(6)^{1/2}\gamma+\frac{80}{21}(6)^{1/2}\tau$	$-\frac{30}{7}\sqrt{3}\beta-\frac{5}{21}\sqrt{3}\gamma+\frac{80}{21}\sqrt{3}\tau$	$5(7)^{1/2}\gamma$
			$\Delta(G)+\frac{6}{7}\beta+\frac{2}{3}\gamma$	$\frac{25}{21}\sqrt{2}\gamma-\frac{110}{7}\sqrt{2}\tau$	$-\frac{5}{7}(42)^{1/2}\gamma+\frac{10}{7}(42)^{1/2}\tau$
				$\Delta(G)-\frac{39}{7}\beta-\frac{101}{21}\gamma+\frac{585}{63}\tau$	$-5(21)^{1/2}\tau$
					$\Delta(G)+3\beta-\gamma-5\tau$
$^1A_2$:	$^1T_1(^1G)$				
	$\Delta(^1G)+3\beta+9\gamma+10\tau$				

Our approach in the analysis of the experimental data may be outlined as follows: The cubic-field parameter, β, and the limiting free-ion multiplet separation between ^3F and ^3P, Δ_P, have been determined from the optical spectra of V^{3+} in corundum. In addition, the trigonal splitting of the excited $^3T_1(^3P)$ state has been measured. Now these data will be supplemented with those from results of the magnetic measurements. The g factors (which are functions of λ and Δ_T) and the Van Vleck temperature-independent susceptibility provide a direct determination of Δ_T. Finally, δ may be obtained from susceptibility measurements in the temperature range 4.2–40°K. Coupling Δ_T with the trigonal-field splitting of the excited $^3T_1(^3P)$, we are able to estimate both trigonal-field parameters. Details of this analysis will be described in the succeeding sections.

2. Reduction of the Energy Matrix

From, for example, McClure's data of the optical spectra[1] we may determine Δ_P and β from the two transitions

$$\begin{aligned}\Delta E\{^3A_2[^3T_1(^3F)];\,^3T_1(^3P)\}&=25\,200\ \text{cm}^{-1},\\ \Delta E\{^3A_2[^3T_1(^3F)];\,^3T_2(^3F)\}&=17\,400\ \text{cm}^{-1}.\end{aligned}\tag{16}$$

After diagonalization of the secular equation (taking into account the shifts in center of gravity by the trigonal field), the results are

$$\Delta_P=9.00\times10^3\ \text{cm}^{-1};\quad \beta=1.27\times10^3\ \text{cm}^{-1}.\tag{17}$$

The proper wave function for the ground state in the cubic field is then obtained by mixing the $^3T_1$ functions

arising from the ^3F and ^3P states through the transformation matrix

$$\begin{matrix}{}^3F \\ {}^3P\end{matrix}\begin{pmatrix} a_1 & a_2 \\ -a_2 & a_1 \end{pmatrix}, \quad a_1=0.959, \quad a_2=0.285. \tag{18}$$

Now the trigonal field, spin-orbit coupling, and magnetic energy may be considered as a small perturbation. In this new representation [after the transformation given in Eq. (18)], the first-order trigonal energies are

$$\begin{aligned} &{}^3T_1({}^3F): \ {}^3A_2=7.6\gamma+12.9\tau, \ {}^3E=-17.3\gamma-6.4\tau, \\ &{}^3T_1({}^3P): \ {}^3A_2=5.4\gamma+17.2\tau, \ {}^3E=0.3\gamma-8.6\tau, \end{aligned} \tag{19}$$

which determine the splittings of the $^3T_1$ states. The second-order elements could be obtained in a similar manner from Table VI and Eq. (18). Further, the principal matrix elements of the spin-orbit energy and magnetic energy are those in Table VI with

$$\begin{aligned} \alpha&=\tfrac{3}{2}a_1^2-a_2^2, \\ \alpha'&=(\tfrac{5}{2})^{1/2}a_1, \\ \alpha''&=a_1^2-\tfrac{3}{2}a_2^2, \end{aligned} \tag{20}$$

where a_1 and a_2 are the mixing coefficients as defined in Eq. (18). In our particular case we have $\alpha=1.29$, $\alpha'=1.52$, and $\alpha''=0.80$.

A Van Vleck transformation[21] is now applied to remove the matrix elements connecting the $^3A_2$ ground state with the upper states in the trigonal field. Such elements arise from the external magnetic field, spin-orbit coupling, and the trigonal potential. Because the lowest ^3E level lies only 1000 cm^{-1} above the ground $^3A_2$, a fourth-order Van Vleck transformation is necessary to adequately reduce the matrix elements between these two states. After this transformation the 3×3 submatrix corresponding to the ground state $^3A_2$ can be isolated. The matrix elements for the cases of external magnetic field perpendicular and parallel to the trigonal field are

$$\begin{aligned}
&\mathfrak{IC}=\mathfrak{IC}_x: \\
&(M_s=0\,|\,M_s=0)=-\mu_0^2[\alpha'^2/\Delta_c+(1-10\alpha^2\lambda^2/\Delta_T^2)\alpha^2/\Delta_T]\mathfrak{IC}_x^2 \\
&\qquad -[2(\alpha\lambda)^2/\Delta_T+(\alpha'\lambda)^2/\Delta_c-2(\alpha\lambda)^4/\Delta_T^3-2(\alpha\lambda)^3/\Delta_T^2], \\
&(M_s=\pm1\,|\,M_s=\pm1)=-\mu_0^2\{\alpha'^2/\Delta_c+[1-(3\alpha^2+2\alpha-4)\lambda^2/\Delta_T^2]\alpha^2/\Delta_T\}\mathfrak{IC}_x^2 \\
&\qquad -[(\alpha\lambda)^2/\Delta_T+(5/2)(\alpha'\lambda)^2/\Delta_c-(\alpha\lambda)^4/\Delta_T^3], \\
&(M_s=0\,|\,M_s=\pm1)=g_\perp\mu_0\mathfrak{IC}_x/\sqrt{2}, \\
&\mathfrak{IC}=\mathfrak{IC}_z: \\
&(M_s=0\,|\,M_s=0)=-\mu_0^2[2\alpha'^2/\Delta_c+2(\alpha+2)^2\alpha^2\lambda^2/\Delta_T^3]\mathfrak{IC}_z^2 \\
&\qquad -[2(\alpha\lambda)^2/\Delta_T+(\alpha'\lambda)^2/\Delta_c-2(\alpha\lambda)^4/\Delta_T^3-2(\alpha\lambda)^3/\Delta_T^2], \\
&(M_s=\pm1\,|\,M_s=\pm1)=\pm g_\parallel\mu_0\mathfrak{IC}_z-\mu_0^2[2\alpha'^2/\Delta_c+(\alpha+2)^2\alpha^2\lambda^2/\Delta_T^3]\mathfrak{IC}_z^2 \\
&\qquad -[(\alpha\lambda)^2/\Delta_T+(5/2)(\alpha\lambda)^2/\Delta_c-(\alpha\lambda)^4/\Delta_T^3], \\
&g_\perp=g-2\alpha^2\lambda/\Delta_T-\alpha'^2\lambda/\Delta_c+\alpha^2(\alpha-1)\lambda^2/\Delta_T^2-\alpha\alpha'^2\lambda^2/\Delta_c\Delta_T+2\alpha^3(\alpha+1)\lambda^3/\Delta_T^3, \\
&g_\parallel=g-(2+\alpha)\alpha^2\lambda^2/\Delta_T^2-4\alpha'^2\lambda/\Delta_c-\alpha\alpha'^2\lambda^2/\Delta_c\Delta_T.
\end{aligned} \tag{21}$$

Here Δ_c denotes the energy spacing between the ground state and the $^3T_2(F)$ as shown in Fig. 1.

3. The Magnetic Susceptibility

The general expression for the paramagnetic susceptibility is[22]

$$\chi=N\frac{\sum\omega_n\{[W^{(1)}(n;n)]^2/kT-2W^{(2)}(n;n)\}e^{-W^0(n;n)/kT}}{\sum\omega_n e^{-W^0(n;n)/kT}}, \tag{22}$$

where the superscript on W denotes those terms which are either linear or quadratic in the magnetic field from application of the perturbation theory discussed in the previous sections. Now the results of Eq. (21) may be substituted in Eq. (22) and we obtain the expressions for the susceptibility

$$\begin{aligned}
\chi_\parallel&=2NB\mu_0^2(g_\parallel^2/kT)\exp(-\delta/kT) \\
&\quad+2NB\mu_0^2\{[2\alpha'^2/\Delta_c+2(\alpha+2)^2\alpha^2\lambda^2/\Delta_T^3] \\
&\quad+2[2\alpha'^2/\Delta_c+(\alpha+2)^2\alpha^2\lambda^2/\Delta_T^3]\exp(-\delta/kT)\}, \\
\chi_\perp&=2NB\mu_0^2(g_\perp^2/\delta)[1-\exp(-\delta/kT)] \\
&\quad+2NB\mu_0^2[\alpha'^2/\Delta_c+\alpha^2(1-10\alpha^2\lambda^2/\Delta_T^2)/\Delta_T] \\
&\quad+4NB\mu_0^2\exp(-\delta/kT) \\
&\quad\times\{\alpha'^2/\Delta_c+\alpha^2[1-(3\alpha^2+2\alpha-4)\lambda^2/\Delta_T^2]/\Delta_T\},
\end{aligned} \tag{23}$$

where

$$B=[1+2\exp(-\delta/kT)]^{-1}.$$

These expressions are valid only as long as the temperature is low enough so that the population of the ^3E state may be neglected. Estimates of the ^3E contribution indicate that the approximation is suitable for $T<600$°K

[21] See, for example, E. C. Kemble, *The Fundamental Principle of Quantum Mechanics* (Dover Publication, Inc., New York, 1958), p. 394.

[22] J. H. Van Vleck, *The Theory of Electric and Magnetic Susceptibilities* (Oxford University Press, London, 1932), p. 182.

if $\Delta_T \sim 1000$ cm^{-1}, which is consistent with the experimental results at high temperature.

IV. ANALYSIS OF DATA

1. Temperature Range 77 to 295°K

For the temperature between 77 and 295°K the expressions for the susceptibility have a simpler form if the exponentials are expanded in powers of δ/kT. The results of such an expansion are

$$\chi_{\parallel}=\tfrac{2}{3}N\mu_0^2\{g_{\parallel}^2[k(T+\delta/3k)]^{-1}+6\alpha'^2/\Delta_c +4(\alpha+2)^2\alpha^2\lambda^2/\Delta_T^3\}\,,$$
$$\chi_{\perp}=\tfrac{2}{3}N\mu_0^2\{g_{\perp}^2[k(T-\delta/6k)]^{-1}+3\alpha'^2/\Delta_c +3\alpha^2[1-4(4\alpha^2+\alpha-2)\lambda^2/3\Delta_T^2]/\Delta_T\}\,. \quad (24)$$

Note that the susceptibilities should follow a Curie-Weiss temperature dependence. Because the trigonal-field splitting Δ_T is much smaller than Δ_c, according to Eqs. (24) the Van Vleck temperature-independent term in $\chi_{\perp}$ is dictated chiefly by Δ_T and should be considerably larger than the temperature-independent component of $\chi_{\parallel}$. In this temperature range the susceptibilities depend strongly upon $g_{\parallel}$, $g_{\perp}$, N, and Δ_T. Changes in λ and δ affect the results only in second order, so in the analysis we use as reasonable estimates $\delta\sim 8$ cm^{-1} and $\lambda/\Delta_T \sim 0.08$.

From the data listed in Table I (Fig. 4), we are able to determine

$$g_{\parallel}/g_{\perp}=(m_{\parallel}/m_{\perp})^{1/2}=1.111\pm 0.003\,, \quad (25)$$

where m_i is the slope of the line χ_i versus $(T+\theta_i)^{-1}$. From the difference in the extrapolated intercept of $\chi_{\parallel}$ and $\chi_{\perp}$ at $T=\infty$, we obtain a good estimate of Δ_T. The quantities Δ_c, α, α' in Eq. (24) are known from the optical data, and the concentration N, appearing as $N\mu_0^2$, follows from

$$N\mu_0^2=(3km_{\parallel})/2g_{\parallel}^2\,, \quad (26)$$

which is 1.85×10^{-5} or 2.72×10^{-6} cgs-emu for the concentrated or dilute sample, respectively. It has been assumed that $g_{\parallel}=1.915$, a value consistent with that obtained by electron spin resonance techniques.[4] If we use the difference in intercept

$$(\Delta\chi)_{T=\infty}=(\chi_{\perp}-\chi_{\parallel})_{T=\infty}=3.9\times 10^{-8} \quad (27)$$

from the extrapolation of the data for the concentrated sample, then

$$\Delta_T=1200\pm 200 \text{ cm}^{-1}\,. \quad (28)$$

TABLE VI. Matrix elements of $H''=\lambda\mathbf{L}\cdot\mathbf{S}+\mu_0(\mathbf{L}+g\mathbf{S})\cdot\mathfrak{IC}$ in cubic representation.[a]

(1) Within the $^3T_1(^3F)$ block

$(0,0|H''|0,\pm1)=\tfrac{1}{2}\sqrt{2}g\mathfrak{IC}_x$
$(0,\pm1|H''|0,\pm1)=\pm g\mathfrak{IC}_z$
$(\pm,0|H''|\pm,0)=\mp\alpha\mathfrak{IC}_z$
$(+,\pm1|H''|+,\pm1)=\mp\alpha\lambda-\alpha\mathfrak{IC}_z\pm g\mathfrak{IC}_z$
$(-,\pm1|H''|-,\pm1)=\pm\alpha\lambda+\alpha\mathfrak{IC}_z\pm g\mathfrak{IC}_z$
$(+,0|H''|+,\pm1)=\tfrac{1}{2}\sqrt{2}g\mathfrak{IC}_x$
$(-,0|H''|-,\pm1)=\tfrac{1}{2}\sqrt{2}g\mathfrak{IC}_x$
$(0,0|H''|\pm,\mp1)=-\alpha\lambda$
$(0,\pm1|H''|\pm,0)=-\alpha\lambda$
$(0,0|H''|\pm,0)=-\tfrac{1}{2}\sqrt{2}\alpha\mathfrak{IC}_x$
$(0,\pm1|H''|+,\pm1)=-\tfrac{1}{2}\sqrt{2}\alpha\mathfrak{IC}_x$
$(0,\pm1|H''|-,\pm1)=-\tfrac{1}{2}\sqrt{2}\alpha\mathfrak{IC}_x$

(2) Between the $^3T_1(^3F)$ block and $^3T_2(^3F)$ block: $(^3T_1|H''|^3T_2)$

$(0,\pm1|H''|0,\pm1)=\pm\sqrt{2}\alpha'\lambda+\sqrt{2}\alpha'\mathfrak{IC}_z$
$(0,\pm1|H''|\pm,0)=\tfrac{1}{2}\sqrt{2}\alpha'\lambda$
$(0,0|H''|\pm,\mp1)=\tfrac{1}{2}\sqrt{2}\alpha'\lambda$
$(0,0|H''|\pm,0)=\tfrac{1}{2}\alpha'\mathfrak{IC}_x$
$(0,\pm1|H''|+,\pm1)=\tfrac{1}{2}\alpha'\mathfrak{IC}_x$
$(0,\pm1|H''|-,\pm1)=\tfrac{1}{2}\alpha'\mathfrak{IC}_x$
$(+,\pm1|H''|+,\pm1)=\mp\tfrac{1}{2}\sqrt{2}\alpha'\lambda-\tfrac{1}{2}\sqrt{2}\alpha'\mathfrak{IC}_z$
$(-,\pm1|H''|-,\pm1)=\pm\tfrac{1}{2}\sqrt{2}\alpha'\lambda+\tfrac{1}{2}\sqrt{2}\alpha'\mathfrak{IC}_z$
$(\pm,\mp1|H''|0,0)=\pm\tfrac{1}{2}\sqrt{2}\alpha'\lambda$
$(\pm,0|H''|0,\pm1)=\pm\tfrac{1}{2}\sqrt{2}\alpha'\lambda$
$(\pm,0|H''|\mp,\mp1)=-\sqrt{2}\alpha'\lambda$
$(\pm,\pm1|H''|\mp,0)=-\sqrt{2}\alpha'\lambda$
$(-,\pm1|H''|0,\pm1)=-\tfrac{1}{2}\alpha'\mathfrak{IC}_x$
$(+,\pm1|H''|-,\pm1)=-\alpha'\mathfrak{IC}_x$
$(+,\pm1|H''|0,\pm1)=\tfrac{1}{2}\alpha'\mathfrak{IC}_x$
$(-,\pm1|H''|+,\pm1)=-\alpha'\mathfrak{IC}_x$
$(\pm,0|H''|\mp,0)=-\alpha'\mathfrak{IC}_x$
$(\pm,0|H''|0,0)=\pm\tfrac{1}{2}\alpha'\mathfrak{IC}_x$

(3) Within the $^3T_2(^3F)$ block

$(0,0|\boldsymbol{L}\cdot\boldsymbol{S}|\mp,\pm1)=\mp\tfrac{1}{2}$
$(0,\pm1|\boldsymbol{L}\cdot\boldsymbol{S}|\pm,0)=\pm\tfrac{1}{2}$
$(+,\pm1|\boldsymbol{L}\cdot\boldsymbol{S}|+,\pm1)=\pm\tfrac{1}{2}$
$(-,\pm1|\boldsymbol{L}\cdot\boldsymbol{S}|-,\pm1)=\pm\tfrac{1}{2}$

(4) Within the $^3T_1(^3P)$ block

$(0,0|\boldsymbol{L}\cdot\boldsymbol{S}|\mp,\pm1)=\alpha''$
$(+,\pm1|\boldsymbol{L}\cdot\boldsymbol{S}|+,\pm1)=\pm\alpha''$
$(-,\pm1|\boldsymbol{L}\cdot\boldsymbol{S}|-,\pm1)=\mp\alpha''$
$(0,\pm1|\boldsymbol{L}\cdot\boldsymbol{S}|\pm,0)=\alpha''$

[a] The two indices in the matrix elements correspond to the second and the third label of the wave functions in Table IV.

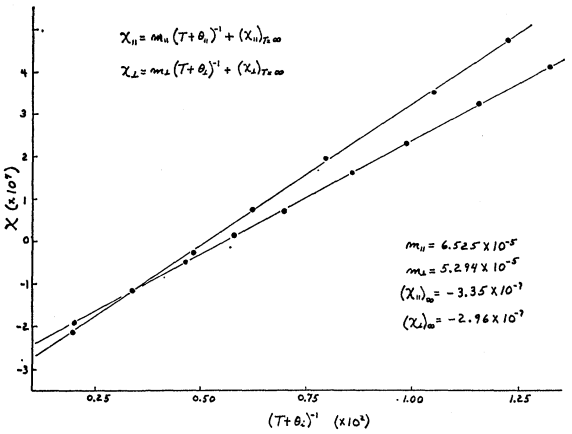

FIG. 4. Magnetic susceptibilities at 77–295°K.

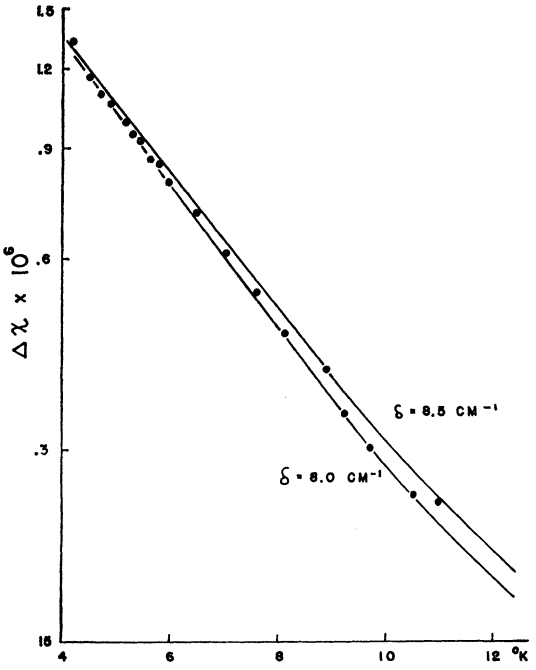

FIG. 5. Magnetic susceptibilities at 4–12°K.

The use of the difference of the Van Vleck term along the two directions has eliminated the diamagnetic contribution of the pure Al_2O_3 crystal. This procedure cannot be checked for consistency by comparison with the dilute sample, because $(\Delta\chi)_{T=\infty}$ is too small for experimental reliability in the latter case.

2. Low-Temperature Susceptibility

The magnetic susceptibility between 4.2 and 12°K is quite sensitive to the zero-field splitting δ of the $^3A_2$ ground state. The temperature-dependent term of $\chi_{\parallel}$ increases as T decreases, goes through a maximum, and then approaches zero as $T\rightarrow 0$. The temperature at which the maximum occurs may be found by differentiating the first term of Eq. (23) with respect to T with the result

$$\delta=(1.017)T\ \text{cm}^{-1}. \tag{29}$$

Since the location of the maximum is dependent only upon δ, it would appear that this is a direct way of determining the zero-field splitting. However, an experimental difficulty arises: when $T<12$°K, the anisotropy torque is so great that the crystal rotates out of position, making a direct measurement of $\chi_{\parallel}$ impossible.

An alternative approach makes use of a measurement of the magnetic anisotropy for temperatures between 4.2 and 35°K. In this temperature range $\Delta\chi=\chi_{\perp}-\chi_{\parallel}$ is large and increases rapidly with decreasing temperature depending upon δ and $g_{\parallel}/g_{\perp}$. We have analyzed the low-temperature data separately in two temperature regions, 4–12°K and 12–35°K. Between 4.2 and 12°K, $\Delta\chi$ can be written, according to Eqs. (23), as

$$\Delta\chi=A[1-(1+R/x)\exp(-x^{-1})]\times[1+2\exp(-x^{-1})]+(\Delta\chi)_{VV}, \tag{30}$$

where $A=2N\mu_0^2g_{\perp}^2/\delta$; $x=kT/\delta$; $R=(g_{\parallel}/g_{\perp})^2$; and $(\Delta\chi)_{VV}$ is the Van Vleck term. Furthermore, for $T<12$°K, $(\Delta\chi)_{VV}$ does not contribute appreciably to the anisotropy and will be neglected. Although it is not immediately obvious from inspection, one finds that $\ln(\Delta\chi)$ shows remarkable linear behavior in x for $0.3<x<0.7$ corresponding to temperatures between 4 and 9°K; the deviation from the average slope is less than 3%. The slope of $\ln(\Delta\chi)$ versus T is

$$\frac{d}{dT}\ln(\Delta\chi)=\frac{d(\Delta\chi)}{dx}\frac{dx}{dT}\Big/\Delta\chi=(k/\delta\Delta\chi)\frac{d(\Delta\chi)}{dx}. \tag{31}$$

From Eq. (30) it is easily shown that for $0.3<x<0.7$,

$$\frac{d(\Delta\chi)}{dx}\Big/\Delta\chi\simeq 3.03 \tag{32}$$

(to within 3%) independent of δ. In Fig. 5 we have plotted $\ln(\Delta\chi)$ against T for different values of δ according to Eq. (30) along with the experimental points. By means of least-squares analysis we obtain

$$\delta=8.3\pm 0.2\ \text{cm}^{-1}. \tag{33}$$

In the temperature range of 12–35°K the values of $\Delta\chi$ are considerably smaller than those at lower temperature, and the contribution of the Van Vleck term to $\Delta\chi$ becomes greater. It is found that the experimental data can be fitted to the theory by choosing $\delta=8.5$ cm^{-1} (see Fig. 6). We see that the values of δ derived from the two temperature regions do not seem to agree perfectly. The major source of error in the evaluation of δ from $\Delta\chi$ at $T=12$–35°K is due to the uncertainty of $(\Delta\chi)_{VV}$ which was obtained from extrapolation of the magnetic data at higher temperatures. When a reasonable amount of deviation of $(\Delta\chi)_{VV}$ is allowed for, the value of δ may

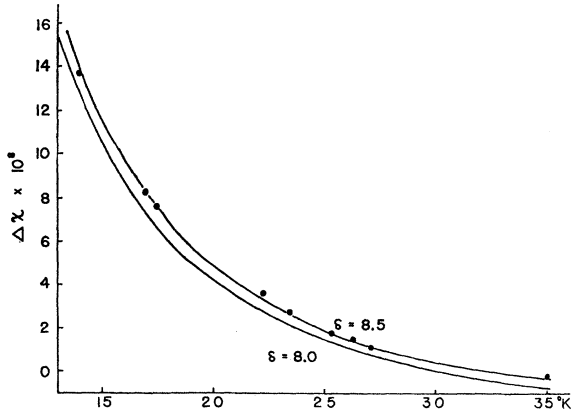

FIG. 6. Magnetic susceptibilities at 12–35°K.

be decreased to 8.4 cm^{-1}. On the other hand, the experimental errors in the temperature measurements limit the accuracy of the result of δ deduced from the susceptibility data at $T<12°K$. We estimate the deviation of δ in this case to be about 0.2 cm^{-1}. Thus, considering the sources of errors in the experimental data, we shall take

$$\delta=8.4 \text{ cm}^{-1} \tag{34}$$

as the most reasonable value with a range of 8.2–8.5 cm^{-1}.

It is also possible to determine δ from the observed data of $\chi_\perp$ at low temperatures. However, the temperature measurements made with the sample in the Faraday balance are less accurate than those in the anisotropy balance. At low temperature this makes the direct measurements of $\chi_\perp$ less reliable than $\Delta\chi$. For this reason the experimental data for $\chi_\perp$ were not used to obtain the zero-field splitting.

3. Temperature above 295°K

At high temperatures we have estimated the contribution of the ^3E state to the susceptibility. For $\Delta_T\sim600$ cm^{-1} we expected a 15% deviation from the Curie dependence obtained for $77°K<T<295°K$. Then for $\Delta_T\sim1000$ cm^{-1} a deviation of 2% should be observed. With $T=500°K$ we were not able to notice any appreciable difference from our Curie dependence. This was interpreted as consistent evidence for a large Δ_T.

4. Crystal-Field Parameters

The two essential pieces of information which were obtained from the experimental data were the ratio $g_{\parallel}/g_\perp$ and δ. Both of these quantities depend explicitly upon the spin-orbit parameter λ and the trigonal splitting Δ_T of $^3T_1$. From Eq. (19) we have

$$\begin{aligned} g_{\parallel}/g_\perp&=1+\epsilon\alpha^2+\epsilon^2[\alpha^4-\alpha^3-\tfrac{1}{2}\alpha^2] \\ &\quad+\epsilon^3[\alpha^6-(3/2)\alpha^5-\alpha^4+\alpha^3] \\ &\quad+(\alpha'^2\lambda/2\Delta_c)[-3+\epsilon(2\alpha-4\alpha^2)], \end{aligned} \tag{35}$$

$$\delta=\lambda[\alpha^2\epsilon-2\alpha^3\epsilon^2-\alpha^4\epsilon^3]-(3/2)\alpha'^2\lambda^2/\Delta_c,$$

where ϵ has been introduced for λ/Δ_T.

Figure 7 shows λ as a function of ϵ for various values of $g_{\parallel}/g_\perp$ and δ. Within a reasonable experimental uncertainty we are able to estimate

$$\begin{aligned} \lambda&\simeq95 \text{ cm}^{-1}, \\ \Delta_T&\simeq1100 \text{ cm}^{-1}, \end{aligned} \tag{36}$$

from the data analysis of the previous section. Figure 7 also shows the dependence of λ upon ϵ through $g_{\parallel}$. Note that these results are consistent with $g_{\parallel}=1.915$ and with the Δ_T we determined from the Van Vleck susceptibility.

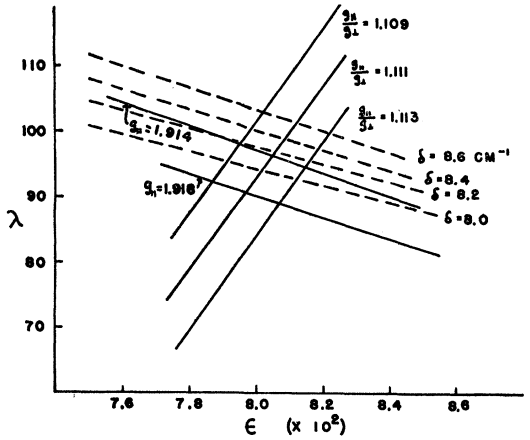

FIG. 7. A plot of λ versus ϵ.

V. DISCUSSION

The values of the spin-orbit coupling constant and Δ_P (the energy difference between the ^3F and ^3P states of the limiting free-ion case) observed for V^{3+} in corundum crystals are smaller than the corresponding quantities of the free ion ($\lambda=104$ cm^{-1}, $\Delta_P=12\,000$ cm^{-1}). Thus, compared to the free ion, λ and Δ_P are reduced by a factor of 1.10 and 1.33, respectively. Using a simple molecular orbital (MO) picture for the bonding between the vanadium and oxygen ions, one may show that the spin-orbit coupling constant in the crystal is approximately equal to that of the free ion divided by the square of the normalization constant of the LCAO MO of the unpaired electron.[16] On the other hand, the $^3F-{}^3P$ separation is governed by the two-electron integral $1/r_{12}$ and should, therefore, be reduced by a factor approximately equal to the fourth power of the normalization constant.[17] We see that this is in good qualitative agreement with the experimental results.

It must be added that the analysis given in the preceding paragraph is somewhat oversimplified. The value of λ obtained in this work is not exactly equivalent to the expectation value of the spin-orbit coupling constant for the $d\epsilon$ (or t_2 in the notation of Pryce and Runciman[3]) state. We determine λ through the second-order perturbation terms, i.e., matrix elements of the spin-orbit operator between the ground state and the excited states which include states originating from the $(d\epsilon)(d\gamma)$ or $(d\gamma)^2$ configurations in addition to $(d\epsilon)^2$. Thus, the "reduction ratio" of λ is not necessarily equal to the square of the normalization constant of the $(d\epsilon)$ LCAO MO. It does turn out, however, that the excited levels which produce the major part of the second-order terms of $(g_{\parallel}/g_\perp)-1$ are associated with the $(d\epsilon)^2$ con-

figuration and, hence, the value of λ reported here should be close to the spin-orbit constant of the $d\epsilon$ state.

If we combine the trigonal splitting of the $^3T_1(P)$ state found in the optical spectrum[1] with our value of Δ_T, it is possible to determine the two trigonal-field parameters. Calculations show that Δ_T depends primarily on γ while the $^3T_1(P)$ splitting is more sensitive to τ. The two parameters are then obtained as

$$\begin{aligned}\gamma &\simeq -38.5\ \text{cm}^{-1},\\ \tau &\simeq -7.3\ \text{cm}^{-1}.\end{aligned} \tag{37}$$

The splitting of the $^3T_1(P)$ state was determined from the separation of absorption maxima in parallel and perpendicular (to the C_3 axis of the crystal) polarization of the $^3T_1(P)$ band.[1] From an analysis of the relative intensity, McClure[1] concludes that such a separation of absorption maxima may not be an accurate measure of the trigonal field. Thus the value of τ given in Eq. (37) is most probably less reliable than γ. Unfortunately, there are not sufficient optical data to test these parameters. Because of the redistribution of intensity due to local tetragonal distortion, the trigonal splitting of the $^3T_2(F)$ state could not be determined experimentally from McClure's spectrum.[1] Nevertheless, using the cubic- and trigonal-field parameters in Eqs. (17) and (37), we have calculated the energies (in cm^{-1}) of the various states as

$$\begin{aligned}&^3A_1\text{: } 17\,100,\\ &^3A_2\text{: } 0,\ 24\,900,\ 35\,900,\\ &^3E\text{: } 1100,\ 17\,600,\ 25\,300,\\ &^1A_2\text{: } 24\,700,\\ &^1A_1\text{: } 9800,\ 21\,000,\ 27\,800,\ 59\,000,\\ &^1E\text{: } 8700,\ 9850,\ 25\,100,\ 28\,300,\ 46\,500.\end{aligned} \tag{38}$$

In this calculation the following values of free-ion energy states were used:

$$\begin{aligned}&^3F-{}^3P=9000\ \text{cm}^{-1},\\ &^3F-{}^1D=7500\ \text{cm}^{-1},\\ &^1D-{}^1G=6000\ \text{cm}^{-1},\\ &^1G-{}^1S=19\,400\ \text{cm}^{-1}.\end{aligned}$$

These calculated energy levels are in satisfactory agreement with the optical spectrum. Here the spin-orbit interaction was not included. The ^3E states will be affected most strongly by the spin-orbit coupling.

It should be interesting to compare the values of γ and τ in Eq. (37) with those calculated from the point-charge model. It is known that if one calculates $A_4{}^0$ in Eq. (6) from the point-charge model and $\langle r^4\rangle$ from the SCF (self-consistent field) atomic wave function, the cubic-field parameter β obtained in this way generally shows poor agreement with experiment. On the other hand, one may fix $A_4{}^0$ by the point-charge model and determine $\langle r^4\rangle$ as a parameter from the experimental value of β. Using such an empirical procedure, McClure was able to account for the trigonal-field splittings of several transition-metal ions in corundum.[1] It is in this sense of an empirical procedure that we are applying the point-charge model. Particularly, the ratio of γ to β is independent of $\langle r^4\rangle$, thus one can avoid the uncertainty associated with the evaluation of $\langle r^4\rangle$. McClure[1] has suggested that the vanadium ions could be slightly displaced from the sites of Al. Using Table IV of Ref. 1, we obtain γ/β as -0.00486 and -0.144, respectively, for a displacement of V^{3+} of 0.00 A and $+0.10$ A from the Al sites. The experimental value for this ratio is -0.0313, supporting McClure's idea of ion displacement.

The situation with τ is more complicated. Presumably Watson's SCF wave function[23] can be used to calculate $\langle r^2\rangle$ yielding 0.460 A^3. However, in the case of Cr_2O_3,[24] the effective value of $\langle r^2\rangle$ which produces the correct trigonal splitting by the point-charge model, is about 70 times smaller than the SCF value. If we adopt this as a criterion for the possible variation of this trigonal parameter, the point-charge model then gives $\tau\simeq 0.42$ $-29.4\ \text{cm}^{-1}$ and $0.73-51.0\ \text{cm}^{-1}$, respectively, for a displacement of 0.00 and 0.01 A of V^{3+}. All these values differ significantly from the experimental value of $-7.3\ \text{cm}^{-1}$.

The reason for this discrepancy is not immediately obvious. From Table IV of Ref. 1, we see that the sign of τ calculated from the point-charge model remains the same for a slight displacement of the substituting ion along the C_3 axis in either direction. It would take a rather large distortion to produce a negative τ. Of course, it is possible that the point-charge model is not suitable for the calculation of this particular parameter. On the other hand, as we have remarked before, the value of $-7.3\ \text{cm}^{-1}$ for τ may not be quite reliable because it was gotten by assuming that the splitting between the absorption maxima (380 cm^{-1}) of the $^3T_1(P)$ band in the two polarizations[1] is entirely due to the trigonal splitting. To investigate this point let us take the lower limit of τ from the point-charge model (which is practically zero). The set of parameters $\gamma=-44.0$, $\tau\simeq 0$ would give $\Delta_T=1100\ \text{cm}^{-1}$, but the trigonal splitting of $^3T_1(P)$ now becomes 236 cm^{-1} with ^3E above $^3A_2$. However, when the spin-orbit coupling and redistribution of intensity due to mixing of states[1] are taken into consideration, the apparent splitting of 380 cm^{-1} as observed in the optical spectrum does not seem unreasonable. This is particularly true if we notice that the band with perpendicular polarization is rather

[23] R. E. Watson, Tech. Rept. No. 12, 1959, Solid State and Molecular Theory Group, MIT, Cambridge, Massachusetts (unpublished).

[24] D. S. McClure, J. Chem. Phys. 38, 2289 (1963).

broad. With the limited amount of information about the crystalline-field parameters at this time, it might be presumptuous to push this point too much further. Nevertheless, for the specific case of V^{3+} in corundum crystals, γ apparently can be accounted for by the point-charge model. Even for τ the result from the empirical point-charge picture is not incompatible with the present optical and magnetic data.

ACKNOWLEDGMENTS

The authors wish to express their appreciation to Professor D. S. McClure for furnishing the crystals to us and for many enlightening discussions. Thanks are also due to Dr. Turner E. Hasty for his assistance and continual interest in this work. We are indebted to Professor J. H. Van Vleck for reading the manuscript and several helpful suggestions.

PHYSICAL REVIEW VOLUME 131, NUMBER 3 1 AUGUST 1963

Electron Paramagnetic Resonance of Cr^{3+} in SnO_2

W. H. FROM
Lincoln Laboratory, Massachusetts Institute of Technology, Lexington, Massachusetts*
(Received 29 March 1963)

The paramagnetic resonance spectrum of the ground state of Cr^{3+} in SnO_2 (cassiterite) was studied at 23.5 and 34.4 kMc/sec. The derived constants of the spin Hamiltonian for the magnetic Z axis coinciding with the crystal c axis are: $|g|=1.975$, $D=+17.3$ kMc/sec, $|E|=8.44$ kMc/sec, and $|A|=42$ Mc/sec.

INTRODUCTION

THE resonance spectrum of the ground state of Cr^{3+} in SnO_2 has been studied to determine the constants of the spin Hamiltonian and to compare these results with those obtained for Cr^{3+} in TiO_2.[1] SnO_2 and the rutile form of TiO_2 belong to the same crystal class, each having tetragonal symmetry. The measured atomic parameters[2] of the two structures, as well as the constants of the spin Hamiltonian, are quite similar.

CRYSTAL STRUCTURE

SnO_2 is a member of the rutile class of crystal structures which are tetragonal and belongs to the D_{4h} point group.[3] The SnO_6 and TiO_6 octahedra differ only slightly from each other as noted below.[2] As in TiO_2, the unit

	SnO_6 (Å)	TiO_6 (Å)
a	4.737	4.594
C	3.185	2.959
$(A-B)$ site 1	2.052	1.944
$(A-B)$ site 2	2.056	1.988

cell consists of two nonequivalent Sn^{4+} sites which can be transformed into each other by a rotation of 90° about the c axis, [001] (Fig. 1). (See Ref. 8.) Even though the SnO_6 octahedra are slightly deformed thus giving local symmetry D_{2h}, i.e., orthorhombic, about an Sn^{4+} site, the resonance data give local symmetry of D_{4h} which is due to the particular way the two nonequivalent sites transform into each other. The two sites are magnetically equivalent when the dc magnetic field lies in the (100) or (010) planes.

EXPERIMENT

The crystals used in the experiment were grown at Lincoln Laboratory under the direction of Dr. T. Reed. The growth habit of the Cr^{3+} doped crystals differed from those doped with other paramagnetic ions. The former had the c axis oriented perpendicular to the crystal-growth axis, whereas with other paramagnetic ions the two coincided. Data concerning the techniques for growing the crystals are described elsewhere.[4]

Nearly all resonance measurements were made at 77°K. A 100 kMc/sec phase-sensitive detection system was used and it, as well as the microwave system, are

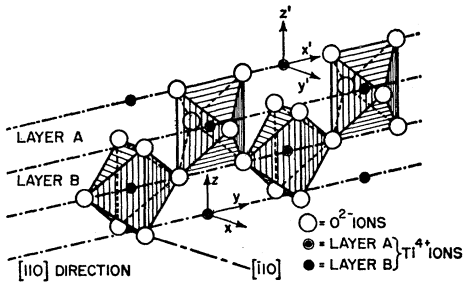

FIG. 1. Crystal structure of SnO_2 depicting the nonequivalent sites for Sn^{4+} and Cr^{3+}. Taken from Andresen's paper with the author's permission (Ref. 8).

* Operated with support from the U. S. Army, Navy, and Air Force.

[1] H. J. Gerritsen, S. E. Harrison, H. R. Lewis, and J. P. Wittke, Phys. Rev. Letters **2**, 153 (1959).

[2] Werner H. Baur, Acta Cryst. **9**, 515 (1956).

[3] R. W. C. Wyckoff, *Crystal Structures* (Interscience Publishers, Inc., New York, 1960).

[4] T. B. Reed, J. T. Roddy, and A. N. Mariano, J. Appl. Phys. **33**, 1014 (1962).